Discovery of Young, Isolated Planetary Mass Objects in the σ Orionis Star Cluster

M. R. Zapatero Osorio,[1*†] V. J. S. Béjar,[1] E. L. Martín,[2,3] R. Rebolo,[1,4] D. Barrado y Navascués,[5,6] C. A. L. Bailer-Jones,[5] R. Mundt[5]

We present the discovery by optical and near-infrared imaging of an extremely red, low-luminosity population of isolated objects in the young, nearby stellar cluster around the multiple, massive star σ Orionis. The proximity (352 parsecs), youth (1 million to 5 million years), and low internal extinction make this cluster an ideal site to explore the substellar domain from the hydrogen mass limit down to a few Jupiter masses. Optical and near-infrared low-resolution spectroscopy of three of these objects confirms the very cool spectral energy distribution (atmospheric effective temperatures of 1700 to 2200 kelvin) expected for cluster members with masses in the range 5 to 15 times that of Jupiter. Like the planets of the solar system, these objects are unable to sustain stable nuclear burning in their interiors, but in contrast they are not bound to stars. This new kind of isolated giant planet, which apparently forms on time scales of less than a few million years, offers a challenge to our understanding of the formation processes of planetary mass objects.

Recent deep photometric and spectroscopic searches have revealed that brown dwarfs, objects unable to stably fuse hydrogen, are very common in star-forming regions, galactic clusters, and the solar neighborhood. Young brown dwarfs in stellar clusters (*1*) have been unambiguously identified with masses ranging from the hydrogen burning limit [75 Jupiter masses ($M_{\rm Jup}$); 1 solar mass is 1047 $M_{\rm Jup}$] down to the deuterium burning threshold (about 13 $M_{\rm Jup}$). This minimum mass limit has been recently proposed (*2–4*) to set the boundary between brown dwarfs and giant planets; while brown dwarfs are capable of fusing deuterium into ^{3}He, one of the lowest threshold energy nuclear reactions, planets never sustain any nuclear burning in their interiors. This nuclear criterion applied to define the term "planet" is independent of any signature based on, so far, rather poorly known formation processes of substellar objects. Radial velocity searches (which already make use of the nuclear definition for separating brown dwarf and planet detections) have shown that brown dwarfs and giant planets with masses ranging from 75 $M_{\rm Jup}$ (the hydrogen burning limit) down to 0.25 $M_{\rm Jup}$ exist in orbits around solar-type and low-mass stars (*5–7*). Whether objects with just a few $M_{\rm Jup}$ or less can form in isolation from stars remains an open issue. Theoretical models describing the fragmentation of collapsing clouds are uncertain regarding the lower mass limit for this process (*8–10*). However, recent observations of the number of objects per mass interval in Orion and other young star-forming regions (*11–14*) suggest that isolated planetary mass objects could also form.

Optical and near-infrared photometry. With the objective of finding isolated planetary mass objects, we carried out a deep photometric survey in the optical and near-infrared wavelengths over an area of 847 arc min^2 around the multiple O9.5-type star σ Orionis (Fig. 1). This survey intentionally covered the same region as the one explored in Béjar *et al.* (*15*), but to much greater sensitivity. According to previous papers (*15, 16*), which describe an analysis of possible reddening using photometric and spectroscopic data of objects in the area, this is a very low extinction region in Orion. Photometry in the *J* band (1.2-μm wavelength) has been collected with the Omega Prime near-infrared camera of the 3.5-m telescope at the Calar Alto Observatory (Almería, Spain) during 27 to 31 October 1998. Optical *I* (870 nm) and *Z* (920 nm) images were acquired with the Wide Field Camera (November 1998) of the 2.5-m Isaac Newton Telescope at the Roque de los Muchachos Observatory (Canary Islands, Spain). Ob-

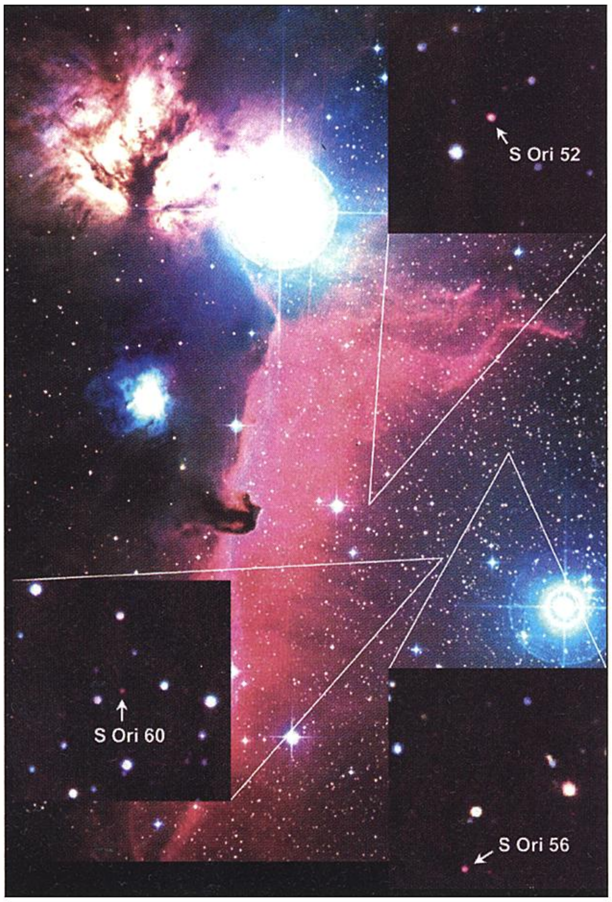

Fig. 1. Location of the σ Orionis star cluster (region around the brightest star in the bottom right side of the figure) and finding charts (45″ by 45″) for three spectroscopically confirmed very young cluster members with masses in the interval 5 to 15 $M_{\rm Jup}$. North is up and east is left. The background image has been taken from ROE/Anglo-Australian Observatory.

[1]Instituto de Astrofísica de Canarias, E-38200 La Laguna, Tenerife, Spain. [2]Division of Geological and Planetary Sciences, California Institute of Technology, MS 150-21, Pasadena, CA 91125, USA. [3]Institute for Astronomy, University of Hawaii, Honolulu, HI 96822, USA. [4]Consejo Superior de Investigaciones Científicas (CSIC), Madrid, Spain. [5]Max Planck Institut für Astronomie, Königstuhl 17, D-69117 Heidelberg, Germany. [6]Universidad Autónoma de Madrid, E-28049 Madrid, Spain.

*To whom correspondence should be addressed. E-mail: mosorio@ll.iac.es
†Present address: Division of Geological and Planetary Sciences, California Institute of Technology, Pasadena, CA 91125, USA.

Table 1. σ Orionis member candidates with masses around and below the deuterium burning mass limit. Coordinates are accurate to ±2″. Uncertainties in the photometric data are given in the text, except for those objects labeled with "‡," for which the uncertainty is a factor 2 larger. RA, right ascension; DEC, declination.

Name	IAU designations	RA (J2000) (hr, min, s)	DEC (J2000) (°, ′, ″)	*I*	*I-J*	*I-K*	Spectral type
S Ori 47*†	S Ori J053814.5-024016	05 38 14.5	−02 40 16	20.53	3.15	4.35	L1.5 ± 0.5
S Ori 50	S Ori J053910.8-023715	05 39 10.8	−02 37 15	20.66	3.12	4.48	
S Ori 51	S Ori J053903.2-023020	05 39 03.2	−02 30 20	20.71	3.50	4.58	
S Ori 52†	S Ori J054009.2-022632	05 40 09.2	−02 26 32	20.95	3.59	4.68	L0.0 ± 0.5
S Ori 53	S Ori J053825.1-024803	05 38 25.1	−02 48 03	21.17	3.28	4.72	
S Ori 54	S Ori J053833.3-022100	05 38 33.3	−02 21 00	21.29	3.30	4.35	
S Ori 55	S Ori J053725.9-023432	05 37 25.9	−02 34 32	21.32	3.10	4.32	
S Ori 56†	S Ori J053900.9-022142	05 39 00.9	−02 21 42	21.74	3.30	4.65	L0.5 ± 0.5
S Ori 57	S Ori J053947.0-022525	05 39 47.0	−02 25 25	21.87	3.24	–	
S Ori 58	S Ori J053903.6-022536	05 39 03.6	−02 25 36	21.90	3.30	5.03	
S Ori 60†	S Ori J053937.5-023042	05 39 37.5	−02 30 42	22.75	3.58	5.07	L4.0 ± 1.0
S Ori 61	S Ori J053852.6-022846	05 38 52.6	−02 28 46	22.78	3.16	–	
S Ori 62	S Ori J053942.1-023031	05 39 42.1	−02 30 31	23.03	3.59	5.36	
S Ori 64	S Ori J053653.3-022414	05 36 53.3	−02 24 14	23.13	3.60	4.51	
S Ori 65	S Ori J053826.1-022305	05 38 26.1	−02 23 05	23.23	3.33	4.41	
S Ori 66	S Ori J053724.7-023152	05 37 24.7	−02 31 52	23.23	3.40	–	
S Ori 67	S Ori J053812.6-022138	05 38 12.6	−02 21 38	23.40‡	3.49‡	–	
S Ori 68	S Ori J053839.1-022805	05 38 39.1	−02 28 05	23.77‡	3.59‡	–	
S Ori 69	S Ori J053918.1-022855	05 39 18.1	−02 28 55	23.89‡	3.64‡	–	

*S Ori 47 lies very close to the deuterium burning mass threshold at the age of the cluster. The *I* photometry is taken from (*15*). †Optical and near-infrared spectroscopy confirms their membership in the σ Orionis cluster.

jects were first identified in the *J* frames and then correlated with their counterparts detected in the *I-Z* optical observations. Raw data were processed with standard techniques in the near-infrared and in the optical (*17*). The limiting *I* (Cousins photometric system) and *J* [UK Infrared Telescope (UKIRT) photometric system] magnitudes of our survey are 23.8 and 21.2, respectively, whereas the 90% completeness magnitudes are estimated at 21.5 and 19.5, respectively. These later values are those at which the distribution of number of stars per magnitude interval in our survey clearly deviate from an exponential law assumed to describe the star counts in the Galaxy. Uncertainties in the *I* and *J* photometry range from about 0.05 mag at completeness to 0.2 mag close to the limit of our search. Additional observations in the *K* band (2.2 μm) with an accuracy of 0.15 mag or better were completed on selected individual targets, using the 1.5-m Carlos Sánchez Telescope at the Teide Observatory (Canary Islands, Spain), the 2.2-m telescope at Calar Alto Observatory, and the 3.8-m UKIRT at the Mauna Kea Observatory (Hawaii, USA).

In the left panel of Fig. 2, we show the *I* versus *I-J* color-magnitude diagram for the 18 candidates found in our survey, which are seen to follow the expected photometric sequence of the σ Orionis cluster. This sequence is defined in the magnitude interval $I = 16$ to 20.5 by previously known objects (*15, 18*) whose membership in the cluster has been confirmed by optical spectroscopy. The coolest of these members is the L1.5-type substellar object S Ori 47 [the newly defined L spectral class (*19, 20*) is the cooler extension to the M-type dwarfs]; because of its age and luminosity, S Ori 47 lies very close to the deuterium burning mass limit (*18*). We concentrate here on 18 candidates with $I > 20.5$ and $I\text{-}J > 3.1$ magnitudes, i.e., fainter and redder than S Ori 47. Their names [based on International Astronomical Union (IAU) rules], coordinates, and photometric data are provided in Table 1. The right panel of Fig. 2 illustrates the *I* versus *I-K* color-magnitude diagram where *K* photometry is available (70% of the sample). Our candidates also define a tight sequence in the *I-K* color, thereby conforming a natural extension of the photometric sequence of the cluster toward very low luminosities. They appear as point sources in the *J* and *K* images with a full width at half maximum (FWHM) of 1.3″, which is the average FWHM of many other objects in the same frames.

Contamination by red galaxies in our sample is expected to be rather low; any extended objects would have been resolved and identified during the visual inspection of the targets. Comparable deep surveys (*21*) searching for extremely red objects (EROs) reveal that galaxies can be distinguished from star-like sources down to $K = 19$ mag in images with typical FWHMs of 1.1″. Unresolved galaxies, quasars, and other extragalactic EROs exhibiting colors as red as those of our candidates should be contributing no more than one to two objects to the list, according to statistics inferred from the Hubble Deep Field survey (*22*). Giant stars reddened and dimmed by interstellar extinction are a negligible source of contamination in our search (*23*) because of the high galactic latitude of the cluster ($b = -17°$). Our presumed planets in σ Orionis should display L-type spectral energy distributions. Therefore, the main source of contamination in our survey is probably due to the L-class, which includes more massive and much older brown dwarfs and low-mass (<0.2 solar mass) stars (*19, 20*) located in foreground and in the direction toward the cluster. From recent discoveries (*19, 24, 25*) by the Deep Near-Infrared Southern Sky Survey (DENIS) and the Two Micron All-Sky Survey (2MASS), it has been established that the sky density of

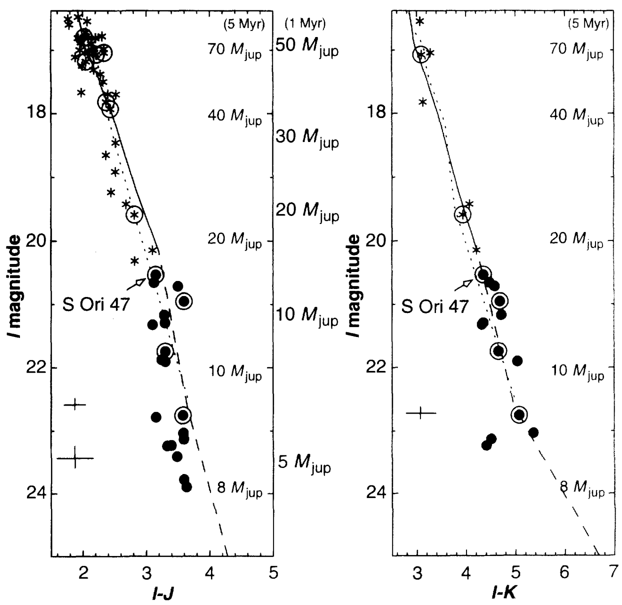

Fig. 2. Optical-infrared color-magnitude diagrams for σ Orionis cluster candidate members found in our *IZJ*, 847 arc min² area survey. Filled circles denote those substellar objects fainter than S Ori 47 whose masses are estimated to be close and below the deuterium burning mass limit (13 times M_{Jup}), whereas the asterisk symbol stands for brown dwarfs above this limit. Those cluster members spectroscopically confirmed are indicated with an open circle around their corresponding symbols. Error bars are given to the left side of the diagrams when they are larger than the symbol size. Overplotted to the data are the theoretical, solar metallicity, 5-My isochrones provided by the Lyon (*30, 31*) group (NextGen models, solid line; dusty models, dashed line) and by the Arizona (*3*) group (dotted line). Masses for two different ages of 5 and 1 My are provided to the right.

objects with early- to mid-L spectral types in the solar vicinity is about 0.0053 objects in a volume of 1 parsec^3 (pc^3), and about 0.0073 objects/pc^3 for the latest L classes. Considering the depth and area coverage of our search in the σ Orionis cluster, we would expect five foreground objects in the L0–L5 spectral interval to be present in our sample, while late-L field dwarf contaminants would be rare ($<$1). This compares with 18 candidate cluster members found by our survey for this L-spectral class. Recent deep optical-infrared searches for EROs (*21*) show a contamination level of galactic L dwarfs consistent with our estimate. We are confident, therefore, that a majority of the candidates in Table 1 are members of the σ Orionis cluster.

Optical and near-infrared spectroscopy. For three of these candidates (plotted with different symbols in Fig. 2) we have obtained follow-up spectroscopy with the Keck I and Keck II telescopes at the Mauna Kea Observatory. Optical spectra for S Ori 52 and S Ori 56 were acquired using the low-resolution imager spectrograph (LRIS) on two nights (5 and 6 January 2000) with a resolution of 1.9 nm and a spectral range from 355.5 to 1125.1 nm. We calibrated in wavelength with the emission spectrum of He Ne Ar lamps. Correction for instrumental response was made using spectra obtained on the same night of a flux standard star (GD140) with fluxes available in the literature. Near-infrared spectroscopy in the wavelength range from 1.4 to 2.5 μm was acquired with the near-infrared camera (NIRC) in February 2000 for S Ori 47 and S Ori 60. Telluric absorptions due to the terrestrial atmosphere were corrected, and flux calibration was performed using the spectrum of the faint photometric standard star FS13 (spectral type G2), observed immediately after the science objects. In Fig. 1, we provide the finder charts for S Ori 52, S Ori 56, and S Ori 60, and Fig. 3 shows their final optical and near-infrared spectra. Spectral types have been estimated under current classification schemes (*20*) in the optical, and by direct comparison with published L-type spectra of field dwarfs in the near-infrared; the values obtained are given in the last column of Table 1. We also considered the slope of the near-infrared spectra in the wavelength region of 1.65 to 1.78 μm (where our data show a reasonable signal-to-noise ratio) for measuring the spectral type of S Ori 60. This slope, which is mainly due to the water vapor absorption in the atmospheres of the objects, becomes noticeable at late types. The claimed 1σ uncertainties in the spectral classification come from the dispersion in the spectroscopic criteria adopted for the calibration. Our data confirm that these candidates are not red giants, background reddened stars, high-redshift quasars, or reddened galaxies, in agreement with our previous analysis of contamination. These candidates display energy distributions within the L-class (L0–L5, atmospheric effective temperatures in the interval 1700 to 2200 K) corresponding to our expectations for young substellar objects members of the σ Orionis cluster. The low resolution and modest signal-to-noise ratio of our spectroscopic data prevent us from carrying out further detailed studies of membership. However, we can estimate the individual membership probabilities in our survey for each of these objects, taking into account their spectral classification and location in the color-magnitude diagrams, the absolute magnitudes and density of L dwarfs (*25*), and the uncertainties of the photometric measurements. These estimations, which were derived using J and K data, are totally independent of evolutionary tracks and mainly rely on the accuracy of photometry, spectral types, and absolute magnitudes of L-type objects. It turns out that S Ori 52 (88%), S Ori 56 (71%), and S Ori 60 (81%) are likely members of σ Orionis, defining a tight spectroscopic cluster sequence down to rather cool spectral types with effective temperatures (*26, 27*) around 1700 K.

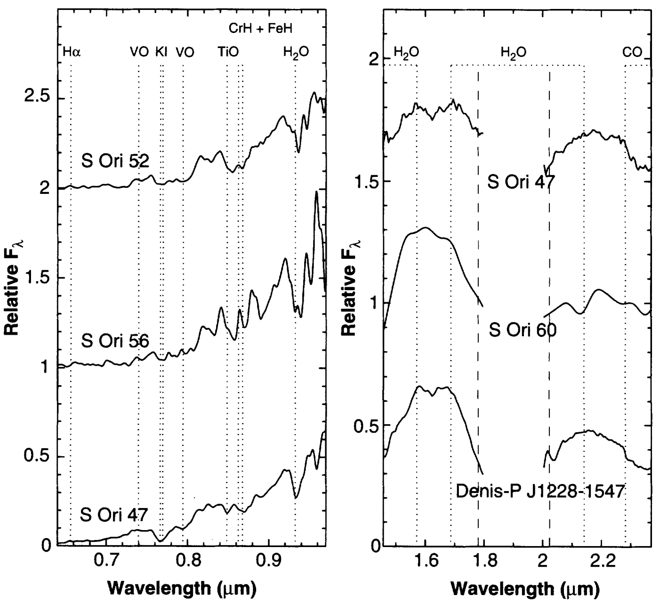

Fig. 3. Optical (left panel) and near-infrared (right panel) Keck spectra for three young isolated planet candidates (S Ori 52, S Ori 56, and S Ori 60) in the σ Orionis cluster. A boxcar smoothing of 5 pixels and a convolution with a 4 σ gaussian kernel has been applied to all the optical spectra and to the near-infrared spectrum of S Ori 60. The main spectroscopic features are indicated. The spectra of S Ori 47 and the field brown dwarf Denis-P J1228-1547 are shown for comparison. In the near-infrared spectra figure, the dashed lines stand for the wavelength range where terrestrial steam absorptions make the spectra unreliable. Spectra are displaced by 1 unity for clarity.

Planetary masses. To estimate the masses of our candidates in Table 1, we have to compare observed magnitudes with those predicted by evolutionary tracks. Mass determinations are then model-dependent and are subject to possible systematic effects arising from the descriptions of the atmospheres and the structure and composition of the interiors. The age of σ Orionis stars and brown dwarfs (including the most massive star in the cluster, σ Orionis) was determined (*28, 29*) to be within 1 million to 5 million years (My). Plotted over the observed photometry of our candidates in Fig. 2 are the 5-My isochrones from the Lyon group (*30, 31*) and from the Arizona group (*3*); all modeis were shifted to the distance of σ Orionis using the Hipparcos satellite-reddened distance modulus (m-M = 7.73, the extinction in the visible wavelengths is around 0.15 mag). The Lyon's tracks facilitate magnitudes and colors in the wavelengths of interest as a function of mass, whereas in order to transform the effective temperatures and luminosities of the Arizona's models into observables, we have considered the bolometric corrections given by the former tracks at a certain age. The "dust-free" next generation (NextGen) Lyon's models are used down to $I = 20$, because we do not expect dusty effects in the atmospheres of M-type cluster brown dwarfs; recent computations of NextGen dusty models are considered for fainter magnitudes. We note that the isochrones reproduce the trend of our near-infrared observations. A direct comparison with the tracks reveals that our candidates could have masses in the interval of 15 to 8 M_{Jup} when we adopt the oldest age of 5 My. Hence, a majority of the candidates are well within the planetary mass domain below the threshold of 13 M_{Jup}. If the cluster is as young as 1 My, the masses of our fainter isolated, giant planets could be as low as 5 M_{Jup}. Those objects, unable to sustain stable thermonuclear reactions in their interiors, radiate energy because they are still undergoing gravitational contraction.

Several sources of uncertainty could affect the mass determinations; however, we have been rather conservative in our estimates. We remark that there is no clear evidence for an infrared excess in our K photometric data that could be associated to individual objects: no dispersion beyond 0.75 mag (ascribed to equal mass binaries) is observed in the color-magnitude diagrams of Fig. 2. The spectra presented here also offer additional proof of the low internal reddening of the cluster. The use of the

Lyon's evolutionary models yields larger masses than other recent models available in the literature (*3, 32*). On the other hand, and in favor of the Lyon's isochrones, it can be argued that they have been successful in fitting the mass-luminosity relation in various optical and infrared passbands (*30*), as well as in predicting coeval ages for the members of several young multiple systems (*33, 34*). The distance and the age of the cluster are important parameters for obtaining masses. Ages not older than 7 to 10 My can be assumed for the massive O9.5-type σ Orionis star, given its present evolutionary status in the main sequence. Adopting the same argument of evolution and based on the photometric and spectroscopic properties of this star, it cannot be located farther than the very young Orion 1b association, i.e., around 450 pc (*29, 35*), to which σ Orionis belongs. The Hipparcos distance we used here is slightly smaller than previous measurements found in the literature, which in turn implies older ages for the cluster sequence. This indeed favors larger mass estimations. In Fig. 4, we illustrate the Herzsprung-Russell diagram (absolute magnitude as a function of effective temperature) for the least massive members of the σ Orionis cluster with available spectroscopy and overplot the Lyon models for two different ages. Effective temperatures were derived from spectral types and averaging the values given by different temperature calibrations (*26, 27*). We note that one of these calibrations (*26*) is based on the same atmosphere models as those used in the evolutionary tracks. The error bars in the temperatures include uncertainties in spectral type and differences in the calibrations. The error bars in the absolute magnitudes take into account a factor 2 uncertainty in the distance to the cluster, corresponding to the Hipparcos error associated to the σ Orionis star. From the diagram, we infer that the location of our objects is consistent with ages as young as 1 to 5 My, in very much agreement with all previous works based on more massive stellar and substellar members. S Ori 47 appears to be overluminous for its spectral type in Fig. 4. A natural explanation is that it could be a nearly equal mass binary, like PPl 15 in the Pleiades (*36*). This would make S Ori 47 less massive than previously estimated (*18*) and, therefore, within the planetary regime of the cluster. We also deduce from the Herzsprung-Russell diagram that S Ori 60 could have a mass in the range 5 to 10 M_{Jup}, which identifies it as the smallest cluster member with planetary masses known so far.

Our findings suggest that the formation of unbound planetary objects can take place within a few million years. This could, therefore, be the result of some rapid gravitational processes and rather short mass accretion stages. The optical spectroscopy does not show any evidence for active accretion (no Hα is detected in emission nor is an infrared excess observed in the K-band of any of the candidates), so apparently they have already reached their final mass. Additionally, the relatively high number of planetary mass candidates discovered in our survey indicates that the population of this very low mass objects is rather numerous, comparable to that of brown dwarfs in the σ Orionis cluster. This, in combination with the results obtained from other searches carried out in different star-forming regions (*11–14*), implies that isolated giant planets form commonly in nature, and may be significantly populating the galactic disc and the solar neighborhood. Standard theoretical models describing the process of collapse of low-mass molecular clouds are unable to explain the formation of numerous, single planetary bodies down to a few M_{Jup}, unless external mechanisms (such as the wind from a nearby supernova) are able to prematurely stop the mass accretion onto the central object. Other alternative processes (*37–39*) have been then proposed, such as multiple cloud fragmentation during collapse, disintegration of massive, gravitationally unstable protoplanetary discs, and core accretion followed by capture of gas in discs around protostars. However, these processes typically produce substellar objects with similar masses or several massive objects that form a multiple-object system. Under these scenarios, efficient mechanisms would have to exist for ejecting planetary objects from their orbits around stars in the relatively short period of a few million years.

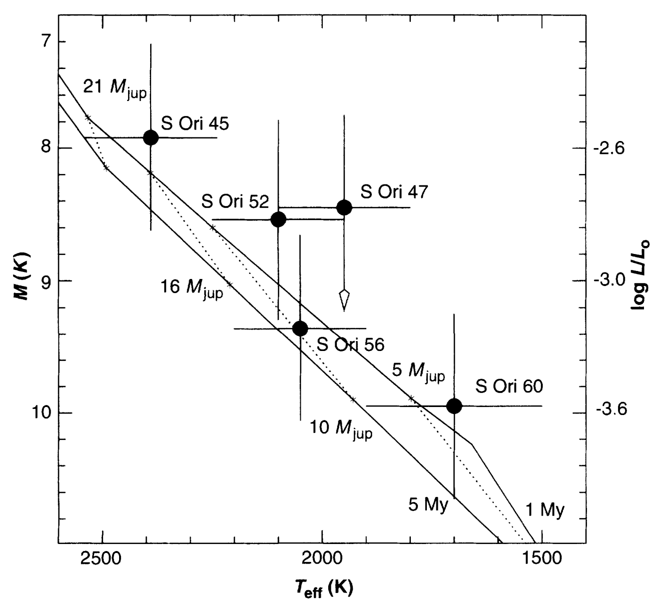

Fig. 4. Absolute $M(K)$ magnitudes as a function of effective temperature for the faintest S Ori objects with available spectroscopy and K photometry. Overplotted are the Lyon's dusty models (*31*) for ages of 1 and 5 My and for temperatures cooler than 2200 K, and dust-free models (*30*) for warmer temperatures. Solid lines are isochrones and dotted lines indicate the evolution of substellar objects of different masses (labeled in M_{Jup}). Luminosities (in solar units) from the models are provided to the right. Vertical error bars account for the uncertainties in the photometry and the distance to the σ Orionis cluster, and horizontal error bars cover different temperature calibrations available in the literature (*26, 27*) for the cool spectral types of the objects. The possible decomposition of S Ori 47 into an equal mass binary is indicated with an arrow. S Ori 60 (10 to 5 M_{Jup}) is the least massive cluster member so far identified.

References and Notes

1. M. R. Zapatero Osorio, in *Very Low Mass Stars and Brown Dwarfs*, R. Rebolo and M. R. Zapatero Osorio, Eds. (Cambridge Univ. Press, New York, in press).
2. D. Saumon *et al.*, *Astrophys. J.* **460**, 993 (1996).
3. A. Burrows *et al.*, *Astrophys. J.* **491**, 856 (1997).
4. G. Basri and G. W. Marcy, *Am. Inst. Phys. Conf. Proc.* **393**, 228 (1997).
5. G. W. Marcy and R. P. Butler, *Publ. Astron. Soc. Pac.* **112**, 137 (2000).
6. M. Mayor and D. Queloz, *Nature*, **378**, 355 (1995).
7. W. D. Cochran, A. P. Hatzes, R. P. Butler, G. W. Marcy, *Astrophys. J.* **483**, 457 (1997).
8. J. Silk, *Astrophys. J.* **214**, 718 (1977).
9. P. Padoan, A. Nordlund, B. J. T. Jones, *Mon. Not. R. Astron. Soc.* **288**, 145 (1997).
10. F. C. Adams and M. Fatuzzo, *Astrophys. J.* **464**, 256 (1996).
11. M. Tamura, Y. Itoh, Y. Oasa, T. Nakajima, *Science* **282**, 1095 (1998).
12. P. W. Lucas and P. F. A. Roche, *Mon. Not. R. Astron. Soc.* **314**, 858 (2000).
13. L. A. Hillenbrand and J. M. Carpenter, *Astrophys. J.* **540**, 236 (2000).
14. J. R. Najita, G. P. Tiede, J. S. Carr, *Astrophys. J.*, in press.
15. V. J. S. Béjar, M. R. Zapatero Osorio, R. Rebolo, *Astrophys. J.* **521**, 671 (1999).
16. T. A. Lee, *Astrophys. J.* **152**, 913 (1968).
17. A total of 24 images of the Omega near-infrared camera were needed to cover the area of 847 arc min^2 around the multiple O9.5-type star σ Orionis in the *J* broad-band filter. Each image actually consisted of 10 co-added 16-s exposures. Raw data both in the optical (*I* and *Z* filters) and near-infrared (*J* and *K* filters) were processed within the IRAF (image reduction and analysis facility) environment. Instrumental aperture magnitudes in the near-infrared were corrected for atmospheric extinction and transformed into the UKIRT system using observations at different air masses of faint standard stars of the list of M. Casali and T. Hawarden [*JCMT-UKIRT Newsl.* **4**, 33 (1992)]. The *I*-band filter was calibrated in the Cousins system by observing photometric standard stars in the optical from the database of A. U. Landolt [*Astron. J.* **104**, 340 (1992)].
18. M. R. Zapatero Osorio, V. J. S. Béjar, R. Rebolo, E. L. Martín, G. Basri, *Astrophys. J. Lett.* **525**, L115 (1999).
19. J. D. Kirkpatrick *et al.*, *Astrophys. J.* **519**, 802 (1999).
20. E. L. Martín *et al.*, *Astron. J.* **118**, 2466 (1999).
21. D. Thompson *et al.*, *Astrophys. J.* **523**, 100 (1999).
22. H. C. Ferguson, M. Dickinson, R. Williams, *Annu. Rev. Astron. Astrophys.*, in press.
23. J. D. Kirkpatrick, J. T. McGraw, T. R. Hess, J. Liebert, D. W. McCarthy Jr., *Astrophys. J. Suppl. Ser.* **94**, 749 (1994).
24. X. Delfosse *et al.*, *Astron. Astrophys. Suppl. Ser.* **135**, 41 (1999).

25. J. D. Kirkpatrick *et al.*, *Astron. J.* **120**, 447 (2000).
26. G. Basri *et al.*, *Astrophys. J.* **538**, 363 (2000).
27. Ya. Pavlenko, M. R. Zapatero Osorio, R. Rebolo, *Astron. Astrophys.* **355**, 245 (2000).
28. S. J. Wolk, thesis, State Univ. of New York at Stony Brook, Stony Brook, NY (1996).
29. A. G. A. Brown, E. J. de Geus, P. T. de Zeeuw, *Astron. Astrophys.* **289**, 101 (1994).
30. I. Baraffe, G. Chabrier, F. Allard, P. H. Hauschildt, *Astron. Astrophys.* **337**, 403 (1998).
31. G. Chabrier, I. Baraffe, F. Allard, P. H. Hauschildt, *Astrophys. J. Lett.*, in press.
32. F. D'Antona and I. Mazzitelli, *Astrophys. J. Suppl. Ser.* **90**, 467 (1994).
33. R. J. White, A. M. Ghez, I. N. Reid, G. Schultz, *Astrophys. J.* **520**, 811 (1999).
34. K. L. Luhman, *Astrophys. J.* **525**, 466 (1999).
35. W. H. Warren and J. E. Hesser, *Astrophys. J. Suppl. Ser.* **36**, 497 (1978).
36. G. Basri and E. L. Martín, *Astron. J.* **118**, 2460 (1999).
37. A. Burkert, M. R. Bate, P. Bodenheimer, *Mon. Not. R. Astron. Soc.* **289**, 497 (1997).
38. A. P. Boss, *Science* **276**, 1836 (1997).
39. P. Bodenheimer, *Astron. Soc. Pac. Conf. Ser.* **134**, 115 (1998).
40. We are indebted to I. Baraffe and the Lyon group for providing theoretical evolutionary tracks prior to publication. We also thank A. Burrows for facilitating an electronic version of his models. We are grateful to C. Gutiérrez and J. Licandro for taking data necessary for calibrating some of the *K* images, and to C. Koresko for making available NIRC spectra of some of the reference objects. This paper is based on observations made with the 2.5-m Isaac Newton Telescope operated on the island of La Palma by the Isaac Newton Group at the Observatorio del Roque de los Muchachos of the Instituto de Astrofísica de Canarias, the Keck I and Keck II telescopes on the Mauna Kea Observatory, the 2.2- and 3.5-m telescopes on the German-Spanish Calar Alto Observatory, the 1.5-m Carlos Sánchez telescope on the Teide Observatory of the Instituto de Astrofísica de Canarias, and the 3.8-m UKIRT telescope on the Mauna Kea Observatory.

6 July 2000; accepted 7 September 2000

REPORTS

Optically Defined Multifunctional Patterning of Photosensitive Thin-Film Silica Mesophases

Dhaval A. Doshi,[1] Nicola K. Huesing,[3] Mengcheng Lu,[1] Hongyou Fan,[1,5] Yunfeng Lu,[4] Kelly Simmons-Potter,[5] B. G. Potter Jr.,[5] Alan J. Hurd,[5] C. Jeffrey Brinker[1,2,5]*

Photosensitive films incorporating molecular photoacid generators compartmentalized within a silica-surfactant mesophase were prepared by an evaporation-induced self-assembly process. Ultraviolet exposure promoted localized acid-catalyzed siloxane condensation, which can be used for selective etching of unexposed regions; for "gray-scale" patterning of refractive index, pore size, surface area, and wetting behavior; and for optically defining a mesophase transformation (from hexagonal to tetragonal) within the film. The ability to optically define and continuously control both structure and function on the macro- and mesoscales is of interest for sensor arrays, nanoreactors, photonic and fluidic devices, and low-dielectric-constant films.

The ability to pattern porous thin films is important for a number of technological applications, including sensor arrays, optics, and microfluidic devices. Mesoporous silicas (*1*) are attractive for such applications because they have internal connectivity and variable density that can be tailored by preparative conditions. Soft lithographic approaches (*2*) have been used to pattern mesoporous films but require long processing times (*3*, *4*) or have been limited to physically defining the presence or absence of discrete isolated regions (*3*, *4*). Rapid patterning of organofunctionalized mesoporous thin films by means of pen lithography, ink-jet printing, and selective dewetting has also been demonstrated recently (*5*), but to date no one has successfully patterned thin-film mesostructure or properties.

Here we report patterning of the mesostructure within a thin film. Our procedure uses evaporation-induced self-assembly to prepare a photosensitive thin-film mesophase containing a photoacid generator (PAG). We then exploit the pH sensitivity of both the siloxane condensation rate and the silica-surfactant self-assembly process to optically define film location, mesostructure, and properties. The procedure begins with a homogeneous solution of silica, surfactant, PAG (a diaryliodonium salt), and HCl (*6*), with initial acid concentration designed to minimize the siloxane condensation rate (*7*, *8*). Preferential ethanol evaporation during dip- or spin-coating (*9*) concentrates the depositing solution in water and nonvolatile constituents, thereby promoting self-assembly (*10*, *11*) into a photosensitive, one-dimensional hexagonal (1-dH) silica-surfactant mesophase. Because it bears a long-chain hydrocarbon, the PAG serves as a cosurfactant during the assembly process, which promotes its uniform incorporation within the mesostructured channels of the 1-dH film.

Irradiation of the PAG at a maximum wavelength (λ_{max}) of 256 nm (reaction 1) results in homolytic or heterolytic photodecomposition to yield the Brønsted superacid, $H^+SbF_6^-$, plus an iodoaromatic compound and organic byproducts (*12*). Thus ultraviolet (UV) exposure of the photosensitive mesophase through a mask creates patterned regions of differing acid concentrations compartmentalized within the silica mesophase (Fig. 1). Co-incorporation of a pH-sensitive dye (ethyl violet) allows direct imaging of these patterned regions as in Fig. 2A, where the yellow (exposed) and blue (masked) regions correspond to pH 0 and pH 2, respectively (*13*).

Suppression of the siloxane condensation rate during film deposition enables several modes of optically mediated patterning. Because acid generation promotes siloxane condensation, selective UV exposure results in patterned regions of more and less highly condensed silica (*14*). Differential extents of siloxane condensation result in turn in differential solubility, allowing selective etching of more weakly condensed regions in aqueous base (0.2

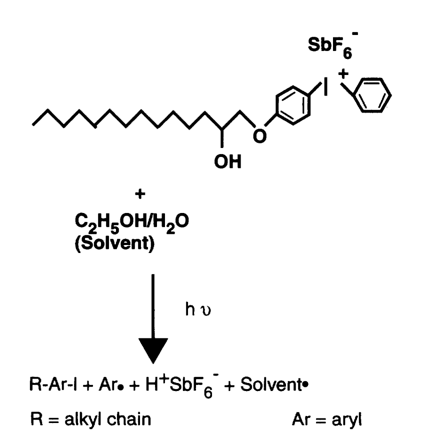

Reaction 1

[1]Department of Chemical and Nuclear Engineering and Center for Micro-Engineered Materials, Advanced Materials Laboratory, University of New Mexico, 1001 University Boulevard SE, Albuquerque, NM 87106, USA. [2]Department of Chemistry, University of New Mexico, Albuquerque, NM 87131, USA. [3]Institute of Inorganic Chemistry, Vienna University of Technology, Vienna, Austria. [4]Applied Materials, Santa Clara, CA 95054, USA. [5]Sandia National Laboratories, Albuquerque, NM 87185, USA.

*To whom correspondence should be addressed. E-mail: cjbrink@sandia.gov